In Vitro Study to Simulate the Intracardiac Magnetohydrodynamic Effect

Waltraud B. Buchenberg,[1]* Wolfgang Mader,[2,3] Georg Hoppe,[1] Ramona Lorenz,[1] Marius Menza,[1] Martin Büchert,[1] Jens Timmer,[2,3,4] and Bernd Jung[1,5]

Purpose: Blood flow causes induced voltages via the magnetohydrodynamic (MHD) effect distorting electrograms (EGMs) made during magnetic resonance imaging. To investigate the MHD effect in this context MHD voltages occurring inside the human heart were simulated in an in vitro model system inside a 1.5 T MR system.
Methods: The model was developed to produce MHD signals similar to those produced by intracardiac flow and to acquire them using standard clinical equipment. Additionally, a new approach to estimate MHD distortions on intracardiac electrograms is proposed based on the analytical calculation of the MHD signal from MR phase contrast data.
Results: The recorded MHD signals were similar in magnitude to intracardiac signals that would be measured by an electrogram of the left ventricle. The dependency of MHD signals on magnetic field strength and electrode separation was well reflected by an analytical model. MHD signals reconstructed from MR flow data were in excellent agreement with the MHD signal measured by clinical equipment.
Conclusion: The in vitro model allows investigation of MHD effects on intracardiac electrograms. A phase contrast MR scan was successfully applied to characterize and estimate the MHD distortion on intracardiac signals allowing correction of these effects. **Magn Reson Med 000:000–000, 2014.** © 2014 Wiley Periodicals, Inc.

Key words: magnetohydrodynamic effect; intracardiac electrograms; electrophysiology; hemodynamics; phase contrast MRI; in vitro model system

INTRODUCTION

The electrical system of the heart can be assessed by means of surface electrocardiography (ECG) and intracardiac electrograms (EGMs) during electrophysiological (EP) studies. Not only can EP disorders be diagnosed but also a better understanding of the mechanisms underlying cardiac arrhythmia can be obtained. In EP examinations, catheters with multiple electrode tips are navigated into the heart to measure EP events. An EP catheter allows three major applications. First, electrical activity of the myocardium can be captured, either in a unipolar (with surface ECG as the reference voltage) or bipolar (with both electrodes within the heart) manner. Second, electrical pulses can be delivered, allowing stimulation of the heart (1). Third, catheter ablation provides the ability to perform nonpharmacological therapy of arrhythmia (2).

Currently, catheters are navigated using fluoroscopy. Hence, patient and medical staffs are exposed to ionizing radiation. Since fluoroscopic images suffer from poor tissue contrast, catheter navigation can be difficult. This may increase both the examination time and the likeliness of complications (3,4).

To overcome these shortcomings, alternative imaging modalities for catheter guidance are desirable. A promising imaging technique is magnetic resonance imaging (MRI), which is based on excitation and relaxation of hydrogen atoms bound in water molecules. It is, therefore, free from ionizing radiation, eliminating the major concern raised by fluoroscopic imaging. Moreover, userdefined imaging planes and various soft tissue contrasts are available to facilitate the navigation of the catheter through anatomical structures (4–7). In addition, scars or lesions on the heart muscle can be depicted on MRI images (4,8). This might allow accurate targeting for catheter ablation and control of the lesion's size for example.

However, combining MRI and EP studies is not straightforward. Due to the strong permanent magnetic field inside the MRI scanner, all devices entering the scanner room have to be nonferromagnetic, including catheters (9). Furthermore, the blood traveling through the magnetic field induces an electrical potential referred to as the magnetohydrodynamic (MHD) effect (10).

The MHD effect is sufficiently large to distort the surface ECG (10–19) and it also alters intracardiac EGMs as shown by Schmidt in his oral presentation of abstract Tse et al. (20). A recently published study by Kainz et al. 2010 (21) compared the MHD effect observed in a tube placed in a low magnetic field of 0.2 T with results obtained by simulations, as well as with an analytical equation, to validate their numerical algorithm for calculating MHD voltages. Recently, in a phantom study properties of the MHD effect predicted by theory such as its velocity dependency, orientation of the electrodes with respect to the external magnetic field of 7 T, and the dependency on the electrode distance were investigated (22). The MHD potential detected by electrodes at the body surface was intended to be applied for synchronizing MR imaging with the cardiac cycle.

[1]Department of Radiology, University Medical Center Freiburg, Medical Physics, Freiburg, Germany.

[2]Department of Physics and Mathematics, Freiburg Center for Data Analysis and Modeling, University of Freiburg, Freiburg, Germany.

[3]Department of Physics, University of Freiburg, Freiburg, Germany.

[4]BIOSS, Centre for Biological Signalling Studies, University of Freiburg, Freiburg, Germany.

[5]Institute of Diagnostic, Interventional and Pediatric Radiology, University Hospital Bern, Bern, Switzerland.

*Correspondence to: Waltraud Buchenberg, Dipl. Phys., University Medical Center Freiburg Radiology—Medical Physics Breisacher Str. 60a D-79106 Freiburg, Germany. E-mail: waltraud.buchenberg@uniklinik-freiburg.de
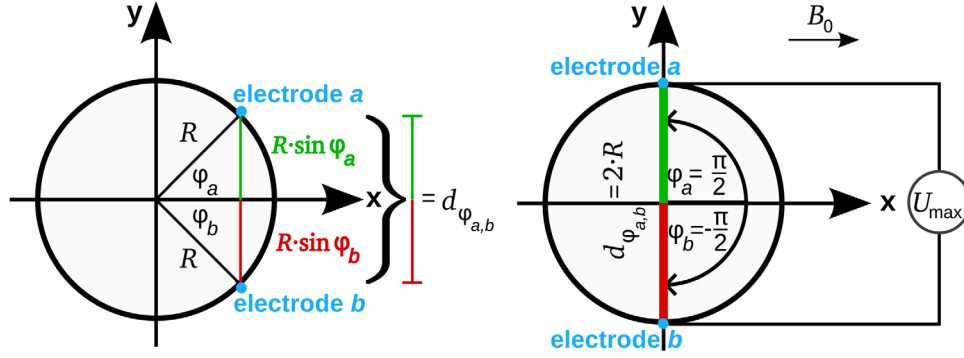
FIG. 1. The cross section of a pipe with radius R is depicted. The flow through the pipe and hence the velocity vector $\vec{v}$ is pointing toward the reader in the z-direction. The external magnetic field B_0 is aligned in the x-direction. On the left, the positions of the electrodes a and b at the pipe wall are shown which can be described by the angles φ_a and φ_b, respectively. The size of the MHD effect only depends on the distance $d_{\varphi_{ab}}$ between the electrodes in the direction perpendicular to the magnetic field and the flow velocity. To calculate the corresponding MHD voltage, $d_{\varphi_{a,b}}$ has be multiplied by the magnetic field B_0 and the mean velocity $\bar{v}_z$. On the right, the electrodes are located at the maximum distance if $\varphi_a = \frac{\pi}{2}$ as well as $\varphi_b = -\frac{\pi}{2}$, and the maximum voltage is induced $U_{max} = 2 \cdot \bar{v}_z \cdot B_0 \cdot R$. [Color figure can be viewed in the online issue, which is available at wileyonlinelibrary.com.]

The aim of this work was the experimental simulation of the MHD effect occurring during EP studies which are carried out in a 1.5 T field, a magnetic field strength commonly used for clinical cardiac MRI and MR guided interventions. As we are considering measurements where both electrodes are within the heart, an MR compatible in vitro model system was designed to provide pulsatile flow conditions which were chosen to reflect the main characteristics of intracardiac flow. EGMs were acquired using devices that are commonly applied in clinical routine during EP studies. MR measurements of flow velocities were also made and investigations into whether these can be used to simulate the effect of intracardiac MHD effect were carried out.

THEORY

Basis of the MHD Effect

Magnetohydrodynamics is a theory combining the Navier–Stokes equations with Maxwell's equations. It describes the behavior of electrically conductive fluids moving in an external magnetic field. The theory can be simplified if low magnetic fields, as applied in MRI, and intracardiac blood flow are considered (23,24). For the problem at hand the induced potential of an axially symmetrical flow in a pipe can be approximated as

$$U(\varphi) = \bar{v}_z \cdot B_0 \cdot R \cdot \sin \varphi \qquad [1]$$

with R, the radius of the pipe, $\bar{v}_z$, the mean velocity of the conductive liquid, and B_0, the external magnetic field (25). A right handed coordinate system is chosen with the flow in z-direction, B_0 in x-direction, and the potential difference ΔU along the y-axis (Fig. 1). The angle with respect to the x-axis is denoted by φ defining the position of an electrode at the circumference of the pipe. The induced potential is then obtained by

$$U := \Delta U = U(\varphi_a) - U(\varphi_b) = \bar{v}_z \cdot B_0 \cdot R \cdot (\sin \varphi_a - \sin \varphi_b). \qquad [2]$$

The variable $d_{\varphi_{ab}} = R \cdot (\sin \varphi_a - \sin \varphi_b)$ is the distance between the electrodes a and b in the direction which is perpendicular to $\vec{B}_0$ and $\vec{v}$ (Fig. 1).

METHODS

The experimental setup for measuring flow velocities and the MHD induced signals in the MR scanner is depicted in Figure 2.
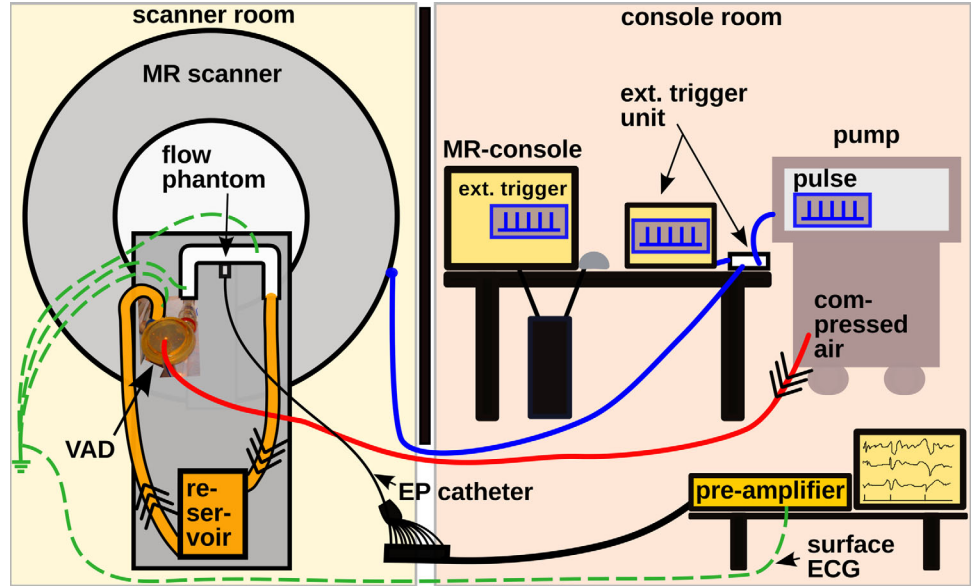
Flow Circuit

The core of the setup was an MR compatible closed flow circuit which consisted of a rigid u-shaped tube (flow phantom, inner diameter: 22.1 mm), a ventricular assist device (VAD, 54 mL, 50 beats per minute, MEDOS, Stolberg, Germany), and a reservoir for liquid.

Rather than attempting to accurately reflect the complex flow within the heart, this set up was designed to emulate the parameters important for the MHD effect caused by intracardiac flow. In this context, it follows from Eq. 1 that the relevant parameter for the MHD effect is the magnitude of the velocity perpendicular to B_0. Therefore, the setup was designed to have pulsatile flow with values of the maximum velocity and mean velocity comparable to intracardiac flow velocities in humans (26–29). Although such intracardiac blood flow is not everywhere perpendicular to B_0 the setup in this work considered the maximum possible MHD effect.

To provide a pulsatile flow within an MR environment the VAD was chosen as an appropriate device. Due to its construction it is not feasible to acquire EGMs within the VAD as the catheter cannot be inserted while the device is pumping. Anyhow, since the VAD serves only as a pump and its inner structure does not reflect the structure of a human heart at all, there is no point to measure within the VAD itself. Furthermore, the location where EGMs were acquired in the flow phantom reflected the main characteristics of intracardiac flow. In addition, the flow phantom provided accurate and reproducible positioning of the multiple electrodes. It was constructed using rapid prototyping and consists of a nonconductive material. However, the nonconductive walls of the flow phantom are not expected to bias the outcome of the

FIG. 2. Experimental setup. The MHD signal was recorded with an EP catheter connected to a preamplifier. The flow was assessed using MR phase contrast measurements for which the MR scanner and the pump were synchronized using an external trigger unit. [Color figure can be viewed in the online issue, which is available at wileyonlinelibrary.com.]

measurement significantly since studies revealed that vessel wall conductivity may be neglected (30).

As a substitute for blood, distilled water with dissolved sodium chloride matching the electrical conductivity of blood was used. The electrical conductivity of the solution was determined using a conductivity meter (Musytec, Bischof Messgeräte CD 24, Neunkirchen-Seelscheid, Germany). It ranged from 0.48 ± 0.02 S/m to 0.64 ± 0.02 S/m at temperatures of 21.5–23.5 °C.

In Figure 3, the tube of the phantom (green) is shown. The catheter (black) was slid into the phantom tube through a port. A guiding ring cut into the wall of the phantom held the catheter in place, preventing possible movement. As schematically shown in Figure 3, the catheter spanned half of the phantom wall's circumference. Ten electrodes were placed on the catheter, as indicated by the numbers in the figure. In the experimental setup the flow velocity $\vec{v}$, the direction along which the MHD voltage was measured, and the external magnetic field $\vec{B_0}$ were mutually perpendicular (Fig. 3).

Measurement Equipment

Measurements were performed on a 1.5 T MR scanner (TIM-Symphony, Siemens, Germany) and an EP station (EP Tracer, CardioTek B.V., Maastricht-Airport) which is a combination of a preamplifier and a computer system for data registration. The MHD potential was measured using a 6 F decapolar EP catheter (10 electrodes of 1.1 mm length with an interelectrode spacing of 5-2-5 mm, Livewire by St. Jude Medical, MN) as applied in clinical routine. Data were recorded by the EP station. The station is designed to record surface ECGs and intracardiac EGMs simultaneously. Since the surface ECG was not present in the experiment, the surface ECG electrodes and the reservoir were connected and grounded (Fig. 2, green dashed lines). This is necessary to provide a reference for the preamplifier during intracardiac measurements.

Velocity Profile of the Flow

As the catheter was not MR compatible, it was replaced by a plastic model of similar size in the flow measure-

ment to avoid imaging artifacts. An external trigger unit was used to synchronize the MR data acquisition and the VAD. The flow profile inside the phantom was assessed by applying a cine phase contrast gradient echo fast low angle shot sequence. The acquired data contained information about the flow velocities in all three spatial dimensions.

The catheter was located in the two-dimensional plane through which the flow was measured (Fig. 3). The MR data was acquired with a temporal resolution of 7.2 ms and
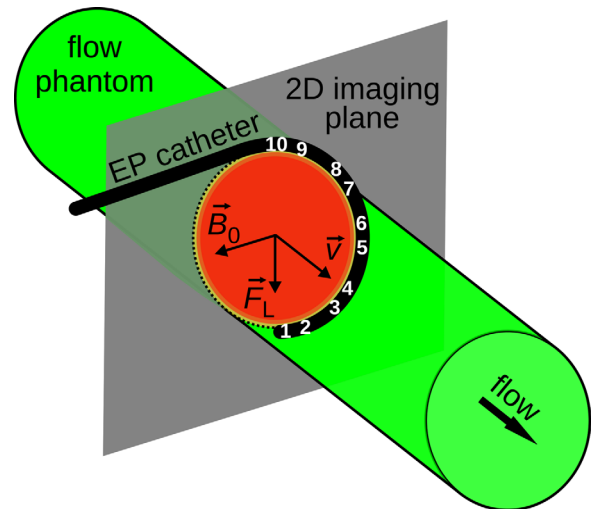

FIG. 3. The EP catheter in black is shown as fitted in the flow phantom's wall. The numbers 1 to 10 mark the positions of the electrodes. The orientation of the catheter with respect to the external magnetic field $\vec{B_0}$, the velocity of the flows $\vec{v}$, and the resulting Lorentz force $\vec{F}_L$ are shown ($\vec{B_0} \perp \vec{v} \perp \vec{F}_L$). Charge carriers are separated due to the Lorentz force. Hence, a potential difference (MHD potential) along the direction of $\vec{F}_L$ arises and is recorded between two different electrodes such as between electrode 1 and electrode 10 (bipolar measurement of the induced MHD voltage). Additionally, the two-dimensional imaging plane of the MR flow measurement is depicted. [Color figure can be viewed in the online issue, which is available at wileyonlinelibrary.com.]

a spatial resolution of $0.9 \times 0.9 \times 6$ mm^3. The velocity sensitivity (31,32) was set to 55 cm/s which was chosen to be higher than the maximum flow expected within the tube.

Two data sets were acquired—one with the flow pump on and one with the pump turned off—and subsequently subtracted to eliminate imaging related velocity offsets (33). Finally, the flow velocities were determined from this corrected data set.

MHD Signal

The time course of the MHD potential was recorded at a 1000 Hz sampling rate. If not stated otherwise, a high-pass filter with a cut-off frequency of 0.05 Hz was applied. A notch filter at 50 Hz was used to remove line noise. Calibration pulses were acquired before and after the signal detection to allow a rescaling of the signals to units of mV.

As shown in Figure 3, the MHD potential was measured in a bipolar manner between the pairs of electrodes 1–10 (channel 1), 2–9 (channel 2), 3–8 (channel 3), 4–7 (channel 4), and 5–6 (channel 5). The distance between electrode pairs of each channel was estimated from the computer aided design plan of the phantom. As depicted in Figure 3, the distances between the electrodes of channel 1 and 2 were approximately equal. From channel 3 to channel 5, the distance between the electrodes decreased. A negative MHD voltage was related to a flow toward the tube phantom corresponding to an emptying of the VAD (systole). In contrast, a positive MHD voltage corresponded to a small back flow occurring in diastole of the VAD cycle when the VAD was refilled.

To investigate the dependency of the MHD voltage on B_0, the MHD signal was measured at different distances from the magnet's isocenter corresponding to different field strengths. The magnetic field at the position of the catheter was determined with a Hall Probe (Lake Shore Model 475 DSP Gaussmeter, Westerville, OH) with an accuracy of 0.15% (manufacturer specification).

To examine the dependency of the MHD signals on the applied high-pass filter, measurements with cut-off frequencies of 0.05 Hz, 0.2 Hz, 40 Hz, and 80 Hz were acquired.

Data Evaluation

The first part of this section describes the data evaluation used to characterize the MHD effect as recorded by intracardiac EGM in the model system. Then, these results are compared to calculations based on MR flow measurements using Eq. 2. The underlying calculations are presented in the second part of this section.

MHD Voltage Signals

Multiple cycles of the MHD signal were acquired during pulsatile flow. The maximum voltage and minimum voltage per cycle were determined at the time points t_1 and t_2. The resulting peak-to-peak voltage per cycle U_{cycle} is depicted in Figure 4. To account for fluctuations of the signal peaks, 10 values of U_{cycle} from consecutive cycles were averaged (denoted by $\bar{U}_{10\ cycles}$). To rule out any dependency of the results on an individual setup of the
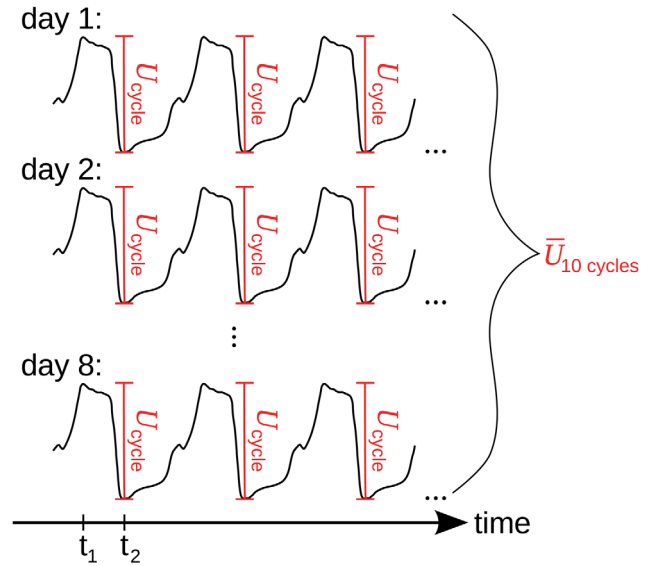

FIG. 4. At an individual day of measuring, the MHD voltage was determined for one cycle U_{cycle} by calculating the difference between the maximum at time point t_1 and the minimum at time point t_2. Multiple consecutive cycles of one measurement were averaged, for example, 10 cycles (denoted by $U_{10\ cycles}$). To eliminate any dependency of the results on an individual setup of the experiment, average results were calculated from data acquired at eight different days ($\bar{U}_{10\ cycles}$). [Color figure can be viewed in the online issue, which is available at wileyonlinelibrary.com.]

experiment, the experiment was newly assembled on eight different days (Fig. 4). The average results thereof are denoted by $\bar{U}_{10\ cycles}$.

Additional measurements were carried out on one of the 8 days to verify that there is a linear relationship between B_0 and $U_{10\ cycles}$. This linear dependency was tested by evaluating a linear regression of the form

$$U_{10\ cycles} = \overline{\Delta\bar{v}}_z \cdot B_0 \cdot d_{\varphi_{ab}} + C \qquad [3]$$

with $\overline{\Delta\bar{v}}_z$ being the average mean velocity difference within the 10 cycles which occurs in the flow at time points of maximum voltages and minimum voltages. Since $d_{\varphi_{ab}}$ was known from the construction plan of the flow phantom, $\overline{\Delta\bar{v}}_z$ could be determined separately for each channel. The parameter C determines an average difference in the signal shift.

The linear dependency of the MHD voltage on $d_{\varphi_{ab}}$ was evaluated for each pair of electrodes in a analogues manner. Since B_0 is known, $\overline{\Delta\bar{v}}_z$ could be determined again from the slope of the linear regression.

MHD Potential Calculation from MR Flow Measurements

The mean through-plane velocity $\bar{v}_z$ was determined for each time point by averaging v_z over the whole cross section of the phantom (Fig. 5, inset). From the construction plan of the phantom the inner radius of the catheter and the position of all electrodes were calculated. From these results, the corresponding $d_{\varphi_{ab}}$ was derived for each of the five pairs of electrodes. The velocity-derived MHD potential was then obtained by
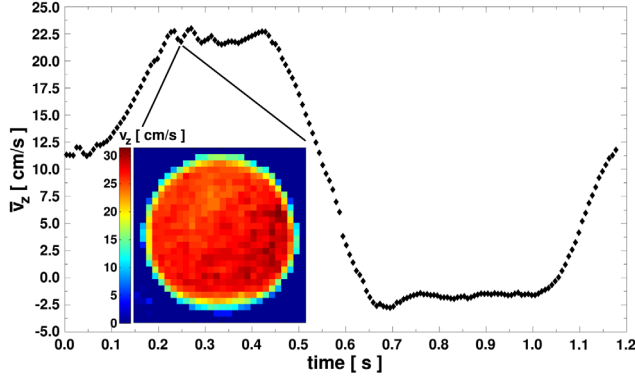
FIG. 5. The mean through-plane velocity $\bar{v}_z$ for one cycle is depicted. The inset shows an example of the velocity distribution occurring during maximum flow inside the flow phantom. The through-plane velocity v_z is color coded in cm/s. The grainy area in the lower left corner originates from the jack for the catheter. [Color figure can be viewed in the online issue, which is available at wileyonlinelibrary.com.]

FIG. 6. The yellow bars show $\bar{U}_{10\ \text{cycles}}$ determined for each channel at $B_0 = 1.5$ T from 8 days of measuring. For comparison $U_{\text{cycle,MRI}}$ calculated from MR flow measurements for each channel is shown in cyan. The errorbars depict the corresponding standard deviations. [Color figure can be viewed in the online issue, which is available at wileyonlinelibrary.com.]

$$U_{\text{cycle,MRI}} = (\bar{v}_z(t_2) - \bar{v}_z(t_1)) \cdot B_0 \cdot d_{\varphi_{ab}} \qquad [4]$$

with $B_0 = 1.5$ T. The time points t_1 and t_2 were the same as used for U_{cycle}. Additionally, time courses of the MHD potential were calculated using

$$U_{\text{MRI}}(t) = \bar{v}_z(t) \cdot B_0 \cdot d_{\varphi_{ab}}. \qquad [5]$$

For a qualitative comparison of the calculated MHD voltage with the measured MHD voltage, 50 consecutive cycles of the measured voltage signal were averaged (denoted by $U_{50\ \text{cycles}}$). To simulate the impact of the filters on the MHD signal, a common filter (Butterworth, fifth order, cut-off frequency: 0.05 Hz, MATLAB [The Mathworks]) was applied to $U_{\text{MRI}}(t)$. This reflects qualitatively the filtering occurring in the MHD voltage measurement.
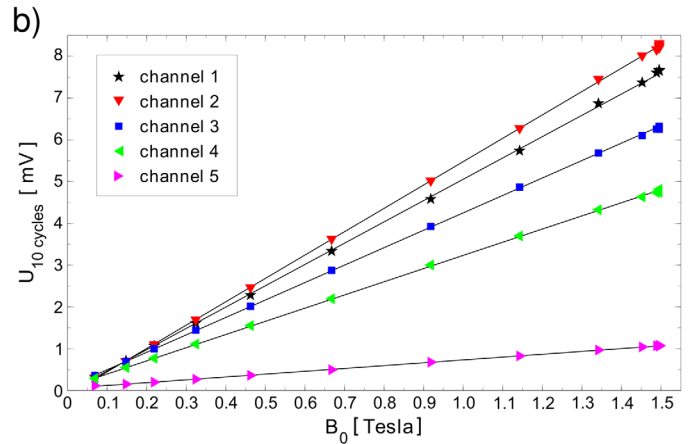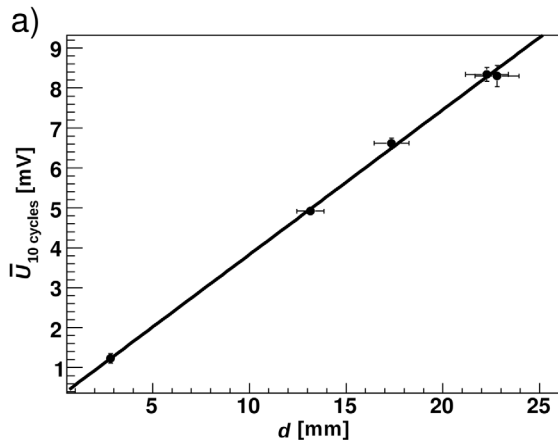
RESULTS

From the MR flow measurements the mean velocity $\bar{v}_z$ of the tube's cross section was derived at different time points within one cycle and can be seen in Figure 5. Although the wave form does not accurately reflect intracardiac flow many of the flow characteristics are similar. The maximum velocity which occurred inside the cross section was 33.3 cm/s. The total flow was 47.6 mL/cycle.

In Figure 6, the MHD voltage $\bar{U}_{10\ \text{cycles}}$ is shown for each electrode pair. The values of channel 1 and channel 2 are almost equal as expected since the electrode distances between the electrode pairs 1–10 and 2–9 are similar. For the other channels, the voltage decreases as the distance between the electrodes decreases. The linear relationship of the MHD voltage with the electrode distance as expected from Eq. 2 was clearly observed (Fig. 7a). The estimated $\overline{\Delta\bar{v}}_z$ from the slope of the linear regression was -24.3 ± 1.0 cm/s (sixth column in Table 1). Similar results for $\overline{\Delta\bar{v}}_z$ were obtained when considering $U_{10\ \text{cycles}}$

FIG. 7. **a:** Linear dependency of the MHD voltage $\bar{U}_{10\ \text{cycles}}$ on the electrode distance $d = d_{\varphi_{ab}}$ of the five channels at $B_0 = 1.5$ T. The line depicts the linear regression. **b:** Linear dependency of the measured MHD voltage $U_{10\ \text{cycles}}$ on different external magnetic fields B_0. The size of errorbars is smaller than the marker size. Lines depict the linear regression. Note this measurement was carried out only at a single day of measuring. [Color figure can be viewed in the online issue, which is available at wileyonlinelibrary.com.]
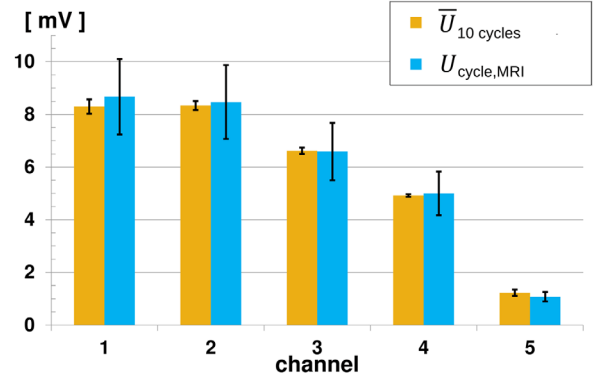
Table 1
$\overline{\Delta\overline{v}}_z$ Determined from the Slope of the Linear Regressions ($U_{10\ cycles}$ vs. B_0 and $\overline{U}_{10\ cycles}$ vs. d) as well as from the MR Phase Contrast Data

$\overline{\Delta\overline{v}}_z$ (cm/s)						
$U_{10\ cycles}$ versus B_0					$\overline{U}_{10\ cycles}$ versus d	MRI
channel 1	channel 2	channel 3	channel 4	channel 5		
-22.4 ± 1.1	-25.1 ± 1.3	-24.1 ± 1.2	-24.0 ± 1.2	-24.0 ± 1.2	-24.3 ± 1.0	-25 ± 4

$\overline{\Delta\overline{v}}_z$ of the MR measurement is strongly dependent on the region of interest used for calculating the mean.

versus B_0 (Table 1, column 1–5). Overall, $\overline{\Delta\overline{v}}_z$ determined throughout the voltage measurements are in good agreement with the MR velocity measurement ($\overline{\Delta\overline{v}}_z = -25 \pm 4$ cm/s). Additionally, the expected linear relationship between $U_{10\ cycles}$ and B_0 is clearly observed (Fig. 7b). The discrepancy between channel 1 and channel 2 is related to variations of $U_{10\ cycles}$ values. As shown in Figure 6 (yellow bars), this effect averages out as multiple measurement days are considered. Hence, channel 1 underestimates $\overline{\Delta\overline{v}}_z$ in this case (see Table 1).

Furthermore, the MHD potential was calculated for all channels based on the MR velocity data using Eq. 4. The values of $U_{cycle,MRI}$ included in Figure 6 are in very good agreement with the corresponding $\overline{U}_{10\ cycles}$ from the measurements with the EP station. Moreover, a qualitative comparison of the measured MHD signal $U_{50\ cycles}$ with the calculated MHD voltage U_{MRI} using Eq. 5 were evaluated. Figure 8 shows this comparison for channel 2 as an example with $U_{50\ cycles}$ shown in red and U_{MRI} shown with black stars. The curves demonstrate a very similar pattern over the entire pumping cycle. The duration of systole and diastole in the two curves are similar. It should be noted that the presence of a high-pass filter in the EP Tracer causes $U_{50\ cycles}$ to be shifted such that the mean value over a cycle is zero. To aid comparison of the temporal evolution of the two curves, U_{MRI} has, therefore, been shifted such that the mean value is zero. Furthermore, the high-pass filter causes a rapid decay of the signal at periods of time where the flow velocities are almost constant (at $t \approx 0.3$–0.45 s as well as 0.8–1.0 s). This characteristic feature is clearly depicted both

in the filtered calculated curve (shown as green triangles) and in the measured curve. Since the filter characteristics of the EP station were unknown, rescaling of the filtered calculated curve by a constant empirical factor of 0.9 provided excellent agreement to the measured data.

Additionally, different high-pass filter settings of the EP station were applied for measuring the MHD signal. The impact of the different filter settings on $U_{10\ cycles}$ was investigated. The percentage value of the fraction

$$f_{\text{cut-off}} = \frac{U_{10\ cycles}(cut-off)}{U_{10\ cycles}(0.05\text{Hz})} \cdot 100\% \qquad [6]$$

with cut-off $\in$ {0.2 Hz, 40 Hz, 80 Hz} is listed in Table 2. Percentage values higher than 100% are possible because of uncertainty in the measurement setup. A drastic reduction of the MHD signal peak-to-peak value occurred when values of 40 Hz or 80 Hz were used for the high-pass filter. The remaining fraction of the signal is about constant for all channels. Filter settings of 40 Hz or 80 Hz are usually clinically used in the bipolar measurements during an EP study.

DISCUSSION

For establishing EP studies in a clinical MR environment, the investigation and characterization of intracardiac MHD potentials which can be also recorded by EP catheters is important. Thus, compared to previous studies (21,22) standard clinical equipment was used in this work to acquire MHD potentials simulated in vitro. It is very difficult to accurately reproduce intracardiac flow by experimental models. The main features of intracardiac flow which are known to highly influence the size of the induced MHD potential are recovered by the established setup. The amplitude of the measured MHD signal was of the same order of magnitude as the intracardiac signals occurring in the left ventricle reported in literature (34). High-pass filters of 40 Hz and 80 Hz, which are commonly used for bipolar EP measurements of intracardiac signals, almost entirely eliminated the MHD signal. However, as described by Josephson (2) filters may alter the shape of intracardiac signals. Thus, the
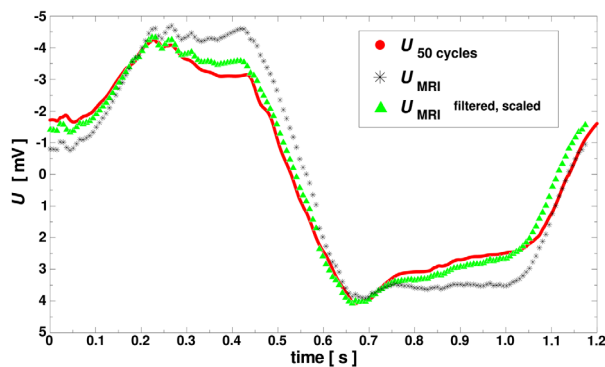

FIG. 8. Qualitative comparison of the measured MHD signal $U_{50\ cycles}$ (●) with the calculated MHD voltage U_{MRI} (∗) for channel 2. For a better comparison of the curves, U_{MRI} was centered in the way that its mean value equals zero. In addition, the curve of U_{MRI} after filtering and scaling is depicted in green (▲). Due to a high sampling rate ● appears as line.

Table 2
Fraction $f_{\text{cut-off}}$ of Eq. 6 Calculated for Each Channel

	channel 1	channel 2	channel 3	channel 4	channel 5
$f_{0.2\text{Hz}}(\%)$	98.9	101.2	103.8	103.1	103.2
$f_{40\text{Hz}}(\%)$	2.4	2.1	2.1	2.1	2.6
$f_{80\text{Hz}}(\%)$	1.0	0.8	0.8	0.9	1.6

application of high-pass filters to eliminate the impact of the MHD effect on intracardiac bipolar signals is a trade-off between effective filtering of the MHD signal and effects altering the EP signals.

The dependency of MHD signals on magnetic field strength and electrode distance were studied. Our results are in excellent agreement with the simplified analytical model (Eq. 2) predicting a linear dependency on field strength and electrode distance (Fig. 7). The latter agrees with the qualitative description presented recently by Frauenrath et al. (22). The focus of their investigation was a different one, since they were interested in finding as large electrode distances as possible to maximize the recognized MHD signal at the body surface. The setup of our study used electrode distances (1–10 mm or more) which are commonly used during EP studies and are well established (2).

As a plausibility check to validate our experimental setup, the MHD voltage signal was used to determine average flow velocities (Eq. 3) which were compared to additionally acquired highly temporal resolved MR flow data. The results of $\overline{\Delta\overline{v}}_z$ for the EP station measurements are in good agreement with the MR velocity measurement. Discrepancies between the averaged MR velocity and the calculated $\overline{\Delta\overline{v}}_z$ of the EGMs could arise from segmentation of the tube area in the MR images or an overestimation of the electrode distance.

The presented flow curve (Fig. 5) and the separately acquired time course of the MHD voltage signal (Fig. 8, •) showed similar curve shapes. This is in agreement with the observations by Frauenrath et al. (22). Therefore, MR phase contrast data may be used as a basis to separate MHD related signal distortions from intracardiac EGMs.

As the MHD voltage scales with the flow velocity and correlates with the temporal changes in the flow, MR phase contrast data could be applied for determining the MHD signal. It was presented by Kainz et al. (21) for a symmetrical static flow profile, that a simple analytical model can be applied to calculate the expected MHD potential. In this work it was shown that the model can also be applied to pulsatile flow. Even with the application of a standard filter and a scaling factor (since the filter properties of the EP system were not available), the actual MHD potential as registered by the EP system could be sufficiently reconstructed.

MR phase contrast data could be easily acquired within a breath-hold period and rapidly evaluated directly at the MR scanner. To determine the position of the catheter with respect to the MR imaging slice and the static external magnetic field real-time catheter tracking and visualization platforms are available such as RTHawk (35) and/or VURTIGO (36). With a region-of-interest close to the catheter location (providing the flow pattern and thus the MHD signal pattern in the area of interest) and a baseline point in the intracardiac ECG cycle (i.e., a zero voltage signal), the intracardiac signal overlaid by the MHD signal could be easily corrected. This would be a fast procedure without the need for an accurate segmentation since no information on the signal amplitude is necessary. However, establishing a visualization platform adjusted to these needs as well as in vivo measurements, for example, with animal models was beyond the scope of this work.

Limitations of the Experimental Setup

Only the static magnetic field of the MR scanner was used for these studies. Therefore, the noise which is additionally superimposed on EGMs during MR measurements was not considered. This issue was solved previously using specifically designed filter circuits (3,7).

The phantom was placed in a 1.5 T field because EP studies in an MR environment are most often carried out at this field strength. At this field strength the retardation of flow due to the MHD effect is small [e.g., even at 5 T the blood flow rate is only reduced by 1.29% (18)] and hence negligible. Applying the presented setup to higher magnetic fields as used for example by Frauenrath et al. (22), would require investigations whether this is still the case.

The flow phantom designed in this work reproduces intracardiac parameters, such as mean and maximum velocities, occurring in the left ventricle of healthy subjects. Nevertheless, it remains an approximation of the actual physiological intracardiac blood flow.

Although blood flow within the great vessels (e.g., in the aortic arch where flow is perpendicular to B_0 and, therefore, will produce an MHD potential) is thought to affect surface ECG measurements, it is not clear what effect this would have on EGM measurements where both electrodes are within the heart. An investigation into this effect was beyond the scope of this experiment.

With our experimental setup using a pulsatile flow, additional oscillating voltage signals are detected if no external magnetic field is present. These signals are poorly reproducible as previously described in the development of a flow meter (25). In the presence of an external magnetic field, there could be other superimposed signals on the pure MHD signal. However, on average peak-to-peak values measured outside the external magnetic field are only about 6% of $U_{10 \text{ cycles}}$. Assembling the setup from scratch on multiple days and averaging the acquired data removes the possible impact on the MHD signals.

Furthermore, the model system could only simulate bipolar measurements since the in vivo surface ECG has to provide the reference for unipolar measurements. However, the model system was focused on bipolar measurements since they are primarily carried out in EP studies.

CONCLUSION

The recorded bipolar MHD signals produced by the in vitro model developed in this work were of the same order of magnitude as the intracardiac signals that would be measured by an EGM of the left ventricle and therefore, this effect should be properly considered. However, the application of sufficiently large high-pass filters prevented the EP system from recording these MHD signals. The dependency of MHD signals on magnetic field strength and electrode distance was well reflected by a simple analytical model of the MHD effect and the acquired MHD signals could be well reconstructed with this model from high temporally resolved MR phase contrast data. Thus, a two-dimensional scan acquired within a breath-hold period and evaluated directly at the MR

scanner could be used to estimate the MHD distortion on intracardiac signals; however, future in vivo studies have to be conducted to develop a suitable workflow for which this work has laid the foundation.

ACKNOWLEDGMENTS

REFERENCES

1. Wellens HJJ. Value and limitations of programmed electrical stimulation of the heart in the study and treatment of tachycardias. Circulation 1978;57:845–853.
2. Josephson ME. Clinical cardiac electrophysiology, techniques and interpretations, 4th ed. Philadelphia: Lippincott Williams and Wilkins, Philadelphia; 2008.
3. Nazarian S, Kolandaivelu A, Zviman MM, et al. Feasibility of real-time magnetic resonance imaging for catheter guidance in electrophysiology studies. Circulation 2008;118:223–229.
4. Lardo AC, McVeigh ER, Jumrussirikul P, Berger RD, Calkins H, Lima J, Halperin HR. Visualization and temporal/spatial characterization of cardiac radiofrequency ablation lesions using magnetic resonance imaging. Circulation 2000;102:698–705.
5. Koopmann M, Marrouche NF. Why hesitate introducing real-time magnetic resonance imaging into the electrophysiological labs? Europace 2013;15:7–8.
6. Lederman RJ. Cardiovascular interventional magnetic resonance imaging. Circulation 2005;112:3009–3017.
7. Nordbeck P, Bauer WR, Fidler F, et al. Feasibility of real-time MRI with a novel carbon catheter for interventional electrophysiology. Circ Arrhythm Electrophysiol 2009;2:258–267.
8. Nordbeck P, Hiller K, Fidler F, et al. Feasibility of contrast-enhanced and nonenhanced MRI for intraprocedural and postprocedural lesion visualization in interventional electrophysiology: Animal studies and early delineation of isthmus ablation lesions in patients with typical atrial flutter. Circ Cardiovasc Imaging 2011;4:282–294.
9. Susil RC, Yeung CJ, Halperin HR, Lardo AC, Atalar E. Multifunctional interventional devices for MRI: A combined electrophysiology/ MRI catheter. Magn Reson Med 2002;47:594–600.
10. Togawa T, Okai O, Oshima M. Observation of blood flow E.M.F. in externally applied strong magnetic field by surface electrodes. Med Biol Eng 1967;5:169–170.
11. Beischer DE, Knepton JJC. Influence of strong magnetic fields on the electrocardiogram of squirrel monkeys (Saimiri sciureus). Aerospace Med 1964;35:939–944.
12. Gaffey CT, Tenforde TS. Alterations in the rat electrocardiogram induced by stationary magnetic fields. Bioelectromagnetics 1981;2: 357–370.
13. Gupta A, Weeks AR, Richie SM. Simulation of elevated T-waves of an ECG inside a static magnetic field (MRI). IEEE Trans Biomed Eng 2008;55:1890–1896.
14. Jekic M, Dzwonczyk R, Ding S, Raman V, Simonetti O. Quantitative evaluation of magnetohydrodynamic effects on the electrocardiogram. In Proceedings of the 17th Annual Meeting of ISMRM, Honolulu, Hawaii, USA, 2009. p. 3795.
15. Kyriakou A, Neufeld E, Szczerba D, Kainz W, Luechinger R, Kozerke S, McGregor R, Kuster N. Patient-specific simulations and measurements of the magneto-hemodynamic effect in human primary vessels. Physiol Meas 2012;33:117.
16. Nijm GM, Swiryn S, Larson AC, Sahakian AV. Extraction of the magnetohydrodynamic blood flow potential from the surface electrocardiogram in magnetic resonance imaging. Med Biol Eng Comput 2008; 46:729–733.
17. Tenforde TS, Gaffey CT, Moyer BR, Budinger TF. Cardiovascular alterations in Macaca monkeys exposed to stationary magnetic fields: Experimental observations and theoretical analysis. Bioelectromagnetics 1983;4:1–9.
18. Tenforde TS, Gaffey CT, Moyer BR, Budinger TF. Magnetically induced electric fields and currents in the circulatory system. Biophys Mol Biol 2005;87:279–288.
19. Weikl A, Moshage W, Hentschel D, Schittenhelm R, Bachmann K. EKG-Veraenderungen durch Einwirkung von statischen Magnetfeldern bei der Kernspintomographie in Magneten der Feldstaerke 0,5 bis 4,0 Tesla. Z Kardiol 1989;78:578–586.
20. Tse ZTH, Dumoulin CL, Watkins R, Byrd I, Schweitzer J, Kwong RY, Michaud GF, Stevenson WG, Schmidt EJ. MRI-compatible voltage-based electro-anatomic mapping system for cardiac electrophysiological interventions. In Proceedings of the 20th Annual Meeting of ISMRM, Melbourne, Australia, 2012. p. 206.
21. Kainz W, Guag J, Benkler S, et al. Development and validation of a magneto-hydrodynamic solver for blood flow analysis. Phys Med Biol 2010;55:7253–7261.
22. Frauenrath T, Fuchs K, Dieringer MA, Özerdem C, Patel N, Renz W, Greiser A, Elgeti T, Niendorf T. Detailing the use of magnetohydrodynamic effects for synchronization of MRI with the cardiac cycle: A feasibility study. J Magn Reson Imaging 2012;36:364–372.
23. Abi Abdallah D, Drochon A, Robin V, Fokapu O. Effects of static magnetic field exposure on blood flow. Eur Phys J Appl Phys 2009; 45:11301.
24. Martin V, Drochon A, Fokapu O, Gerbeau JF. Magnetohemodynamics in the aorta and electrocardiograms. Phys Med Biol 2012;57:3177.
25. Kolin A. An alternating field induction flow meter of high sensitivity. The review of scientific instruments 1945;16:109–116.
26. Buchenberg WB, Markl M, Bauer S, Bock J, Lorenz R, Jung BA. Dual venc phase contrast MRI for simultaneous assessment of blood flow and cardiac motion. In Proceedings of the 19th Annual Meeting of ISMRM, Montréal, Canada, 2011. p. 3303.
27. Eriksson J. Quantification of 4D left ventricular blood flow in health and disease. Ph.D. Thesis, Linköping University, 2013.
28. Föll D, Taeger S, Bode C, Jung B, Markl M. Age, gender, blood pressure, and ventricular geometry influence normal 3D blood flow characteristics in the left heart. Eur Heart J Cardiovasc Imaging 2013;14: 366–373.
29. Fyrenius A, Wigström L, Ebbers T, Karlsson M, Engvall J, Bolger AF. Three dimensional flow in the human left atrium. Heart 2001;86:448–455.
30. Abi Abdallah D, Drochon A, Robin V, Fokapu O. Magnetohydrodynamic flow of blood: Influence of the simplifying assumptions in calculations. J Biomech 2008;41:S269.
31. Lotz J, Meier C, Leppert A, Galanski M. Cardiovascular flow measurement with phase-contrast MR imaging: Basic facts and implementation1. Radiographics 2002;22:651–671.
32. Markl M. Velocity encoding and flow imaging. Available at: http://ee-classes.usc.edu/ee591/library/Markl-FlowImaging.pdf, 2005. Accessed on August 28, 2013.
33. Chernobelsky A, Shubayev O, Comeau CR, Wolff SD. Baseline correction of phase contrast images improves quantification of blood flow in the great vessels. J Cardiovasc Magn Reson 2007;9: 681–685.
34. Cassidy DM, Vassallo JA, Marchlinski FE, Buxton AE, Untereker WJ, Josephson ME. Endocardial mapping in humans in sinus rhythm with normal left ventricles: Activation patterns and characteristics of electrograms. Circulation 1984;70:37–42.
35. Santos JM, Wright GA, Pauly JM. Flexible real-time magnetic resonance imaging framework. In Engineering in Medicine and Biology Society, 2004. IEMBS'04. 26th Annual International Conference of the IEEE, San Francisco, California, USA, Vol. 1. 2004. pp 1048–1051.
36. Radau PE, Pintilie S, Flor R, Biswas L, Oduneye SO, Ramanan V, Anderson KA, Wright GA. VURTIGO: Visualization platform for real-time, MRI-guided cardiac electroanatomic mapping. In Statistical Atlases and Computational Models of the Heart, Imaging and Modelling Challenges. Berlin: Springer; 2012. pp 244–253.